ChemSusChem

Research Article
doi.org/10.1002/cssc.202301362

Chemistry Europe
European Chemical Societies Publishing

www.chemsuschem.org

Special Collection

Effect of Guest Solvents on the Ionic Conductivity and Electrochemical Performance of Metal-Organic Framework-Based Magnesium Semi-Solid Electrolytes

Hagar K. Hassan,*[a, b, c, d] Paul Hoffmann,[c] and Timo Jacob*[a, b, c]

Developing suitable electrolytes is crucial for the advancement of rechargeable magnesium batteries. Recently, metal-organic frameworks (MOFs) have shown a great interest in the field of solid electrolytes for metal ion batteries. However, the ionic conductivity as well as the electrolyte stability in the presence of Mg electrodes are shown to be strongly dependent on the guest solvent used to solvate Mg salts in MOFsSEs. Our measurements showed that full evacuation of the MOF structure before semi-solid electrolytes (sSEs) preparation is crucial for achieving relatively low Mg overpotentials regardless of the ionic conductivity values. Moreover, the behavior of the anode/MOFsSEs interfaces (MOF: α-$Mg_3[HCOO]_6$; Mg salt : $MgCl_2$-$Mg[TFSI]_2$ (1 : 1 wt%); guest solvent: acetone, DMF, DEG, DME and tetraglyme) was investigated by EIS, CV and galvanostatic measurements. The current comparative study of the electrochemical deposition processes of magnesium from MOFsSEs revealed that magnesium deposition/dissolution reactions vary depending on the MOF structure, the guest anion species as well as the nature of the guest solvents.

Introduction

Magnesium-ion batteries (MIBs) are emerging as promising alternatives to traditional lithium-ion batteries due to the abundance of magnesium, which offers a low-cost and environmentally friendly alternative to lithium.[1,2] MIBs have several advantages over lithium-ion batteries, including higher theoretical capacity, better safety, and a lower risk of dendrite formation.[2] However, the passivation of the Mg anode in most known liquid electrolytes is one of the main obstacles for the development of Mg-ion batteries. To solve this problem, new electrolytes must be developed. Batteries based on solid-state electrolytes (SEs) or semi-solid electrolytes (sSEs) are promising alternatives to traditional liquid electrolyte batteries due to their higher energy density, improved safety, and longer lifespan making them better suited for solving problems of Mg-ion batteries.[1] Metal-organic frameworks (MOFs) have emerged as promising material class to be used in solid-state batteries (SBs) due to their high surface area, tunable pore sizes, and versatile chemistry.[3–6]

In addition, previous studies have investigated MOFs as promising matrices for semi-solid electrolytes (sSEs) in lithium, sodium, and magnesium-ion batteries.[7–10] Although several reports investigated the effects introduced by guest metal salts (anion species) or the MOF structure on the ionic conductivity of the resulting MOFs-based sSE, there still remain various questions about the impact of guest solvents inside the cavities of MOFs on the measured ionic conductivities. For example, Zhao *et al.*[11] tried using different MOFs as SEs for lithium-ion batteries. They could achieve ionic conductivities in a range of 10^{-6}–10^{-3} S cm^{-1} with a cation transference number of 0.4–0.6. On the other hand, Long *et al.*[12] studied the effect of extending the organic linker and changing the guest magnesium salts on the ionic conductivity of MOF-based sSEs. Based on their work, the $MgCl_2$-$Mg(TFSI)_2$ mixture provided the optimal ionic conductivity compared to other salts used in their studies. Additionally, the expanded structure Mg_2(dobpdc) (dobpdc^{4-} = 4,4′-dioxidobiphenyl-3,3′-dicarboxylate) showed an enhanced ability for incorporating larger amounts of Mg salts into its pores compared to Mg_2(dobdc) (dobdc^{4-} = 2,5-dioxidobenzene-1,4-dicarboxylate). On the other hand, Miner *et al.*[13] tested the magnesium ion conductivity of a Cu-azolate MOF and received high conductivities (10^{-5}–10^{-4} S cm^{-1}), a relatively low activation energy for ion migration, and the ability to immobilize anions.

[a] Dr. H. K. Hassan, Prof. T. Jacob
Department of Electrochemistry II and Theory I
Helmholtz Institute of Ulm (HIU)
Helmholtz Str. 11, 89081 Ulm (Germany)

[b] Dr. H. K. Hassan, Prof. T. Jacob
Karlsruhe Institute of Technology (KIT)
P.O. Box 3640, 76021 Karlsruhe (Germany)
E-mail: hagar.ibrahim@kit.edu

[c] Dr. H. K. Hassan, P. Hoffmann, Prof. T. Jacob
Institute of Electrochemistry
Ulm University
Albert-Einstein-Allee 47, 89081 Ulm (Germany)
E-mail: timo.jacob@uni-ulm.de

[d] Dr. H. K. Hassan
Faculty of Science
Cairo University
12613, Cairo (Egypt)

Supporting information for this article is available on the WWW under https://doi.org/10.1002/cssc.202301362

Special Collection This publication is part of a joint Special Collection dedicated to Post-Lithium Storage, featuring contributions published in Advanced Energy Materials, Batteries & Supercaps, and ChemSusChem.

Although these are superior results for MOFs-sSEs, there is still a question mark on the reported ionic conductivities and the dependence on the presence of high guest-solvent contents inside the cavities of MOFs. For instance, research on non-aqueous Mg liquid electrolytes showed a strong influence of the solvent on the ability of the electrolyte to successfully and reversibly deposit Mg as well as on the nature of the deposited species. Gewirth et al.[14] studied the effect of the solvent on Mg deposition and stripping from a series of $MgCl_2$-MCl_x mixtures and showed that the ability of the co-salt and the solvent to form multimeric Mg species is crucial for a successful Mg deposition and stripping. They also hypothesized that six-coordinated Mg dimers facilitate Mg electrodeposition and -dissolution in the $MgCl_2$-$AlCl_3$ electrolyte, consequently, Mg deposition/stripping processes are favorable from $MgCl_2$-$AlCl_3$ mixtures in mono- and diglymes but not possible with tri- and tetraglymes. Drews et al.[15] studied the influence of different solvents on the battery performance for tetrakis(hexafluoroisopropyloxy)borate electrolyte salts. They observed that the deposition reaction for mono-, tri- and tetraglyme is strongly dependent on the initial desolvation of the Mg cations, whereas the influence of desolvation on the plating reaction is minor for diglyme and tetrahydrofuran, with a high recommendation on using diglyme as the optimal solvent. All the previous reports suggest that the performance of the Mg electrolyte is highly-sensitive to any changes in its components, including anions, co-salt, and solvent. In general, one cannot say that a certain solvent is generally preferred over another without taking all the other electrolyte's components into consideration. However, all of the reports summarized above have one common conclusion: the desolvation of Mg ions seems to be the limiting step that controls the Mg deposition process, which is mainly dependent on the solvent. Thereby, studying the influence of solvent in any proposed Mg electrolyte is highly important.

In our previous report,[16] we presented mixed MOFs of different structure and crystallinity (amorphous Mgbp3dc (bpdc-2 = 2,2'-bipyridine-3,3'-dicarboxylic acid) and crystalline α-$Mg_3[HCOO]_6$) with an advanced approach to minimize the guest solvent content in the MOFs' cavities. This MOF mixture exhibited a high ionic conductivity of 3.8×10^{-5} S cm^{-1} at 30 °C compared to 1.1×10^{-6} S cm^{-1} for single phase crystalline α-$Mg_3[HCOO]_6$. Additionally, it showed a reversible Mg deposition/stripping behavior and good compatibility with Mg electrodes. This indicates that the MOF's structure also affects the solvation and consequently the ionic conductivity. These previous studies on the effects of the MOF structure and the guest salt on its ionic conductivity inspired us to further investigate the effect of the guest solvent independently in order to fully understand the role of each component in MOF-based Mg semi-solid electrolytes (MOFsSEs). In this context, the effect of the type and content of the guest solvent on the ionic conductivity of MOFsSEs is investigated. Here, α-$Mg_3[HCOO]_6$ has been chosen as MOF matrix for Mg salts due to its simpler structure, high stability against temperature, pressure, and chemicals, ease of synthesis, and low cost.[17–19] These properties make α-$Mg_3[HCOO]_6$ a well-suited model system for investigating the role of the guest solvent and to avoid any contribution from the open framework provided by the previously reported mixed MOF-sSEs.[16]

Results and Discussion

The α-$Mg_3[HCOO]_6$ metal-organic framework is a highly porous structure that is easily synthesized by a hydrothermal reaction of magnesium nitrate and formic acid in dimethylformamide (DMF) as described in the experimental section. Therefore, after growth of the MOF structures, the DMF molecules fill their cavities in a way that hinders their further uptake. Sometimes, it is difficult to remove these solvent molecules by heating because of the possibility of the structure to collapse upon heating. Thanks to the high thermal stability of α-$Mg_3[HCOO]_6$, the evacuation process can be easily performed without altering the framework structure. This step is crucial to activate the MOFs for any desired application. In order to investigate the influence of the remaining DMF molecules inside the MOF cavities, the as-synthesized α-$Mg_3[HCOO]_6$ framework was evacuated at different temperature and pressure conditions. PXRD, ^{1}H-NMR, and TGA were used to investigate the phase purity as well as the complete evacuation process. As shown in Figure 1a, α-$Mg_3[HCOO]_6$ was successfully synthesized in good agreement with the reference card number 01-084-7581. It has a monoclinic structure with a space group of P21/*n*, consisting of four crystallographically non-equivalent magnesium sites, twelve oxygen sites, six hydrogens, and six carbon sites.

As shown in Figure 1b, the MOF framework is constructed by connecting 1D chains of MgO_6 edge-sharing polyhedrals of Mg1/Mg3 with corner-shared polyhedrals of Mg2 and Mg4 along two directions through Mg1 polyhedrals, resulting in a 1D zigzag channel along the crystalline axis *b*.[20]

The crystallinity of α-$Mg_3[HCOO]_6$ is enhanced after thermal activation compared to the as-synthesized material. No significant differences between the XRD patterns of α-$Mg_3[HCOO]_6$ activated under different pressure have been observed. However, a decrease in the peak intensities was observed when the evacuation time exceeded 48 h at 10^{-5} mbar, instead 24 h were already sufficient to obtain highly-crystalline solvent-free MOFs. As shown in Figure 1c, ^{1}H-NMR spectroscopy of the activated α-$Mg_3[HCOO]_6$ under 10 mbar at 130 °C revealed the presence of some remaining DMF molecules as an indication of an incomplete evacuation. Meanwhile, the evacuation process under higher vacuum (10^{-3}–10^{-5} mbar) is mandatory to obtain solvent-free α-$Mg_3[HCOO]_6$. TGA curves of as-synthesized, evacuated at 10 mbar and evacuated at 10^{-5} mbar MOF samples are shown in Figure 1d. The activated α-$Mg_3[HCOO]_6$ at 10 mbar showed a mass loss from 240 to 300 °C for the removal of the remaining DMF molecules. The MOF that was evacuated at 10^{-5} mbar did not show any mass loss until 420 °C, indicating the successful removal of all solvent molecules from the frameworks. The mass loss from 420 °C to 460 °C is due to the removal of formate ligands and the collapse of the framework indicating that α-$Mg_3[HCOO]_6$ has a very high thermal stability up to 420 °C. The small mass loss from 460 to 520 °C is due to

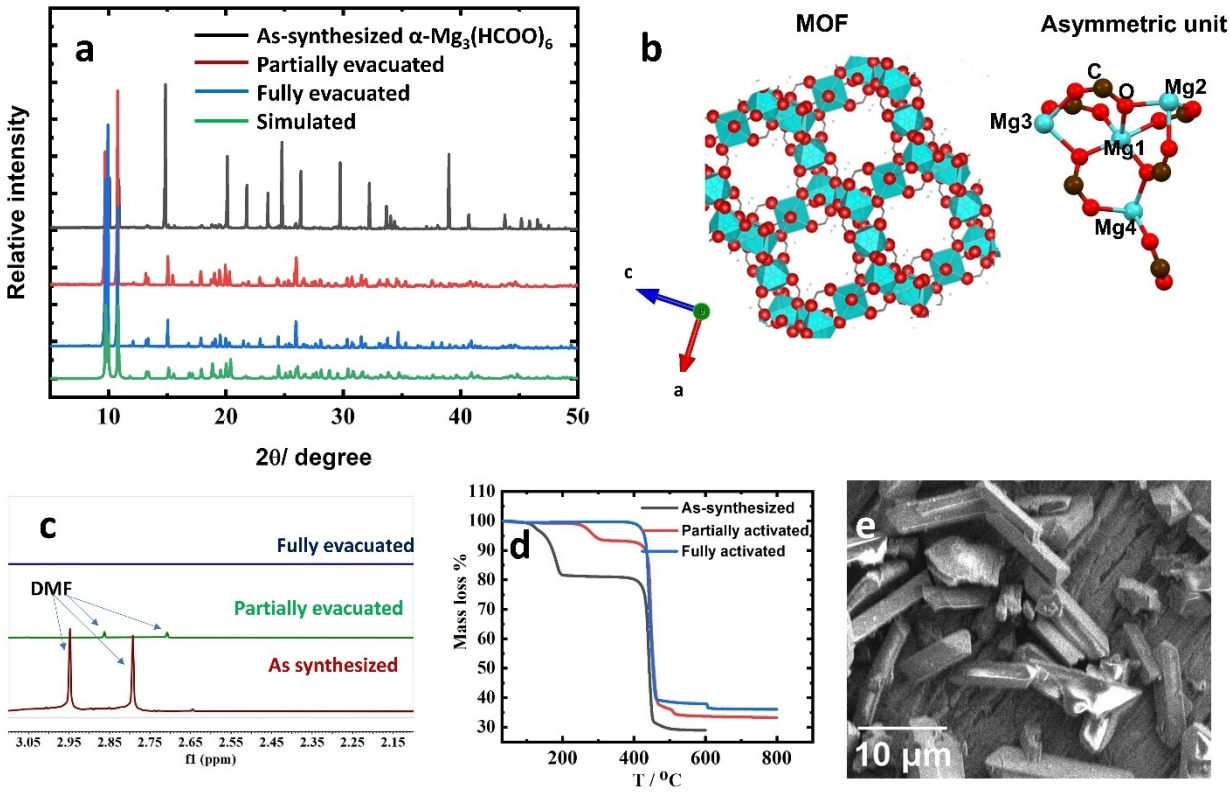

Figure 1. a) XRD of α-$Mg_3(HCOO)_6$, b) 3D-structure of the fully-evacuated MOF showing its pores and its asymmetric unit cell, c) 1H-NMR of as-synthesized, partially evacuated and fully evacuated α-$Mg_3(HCOO)_6$, d) TGA of as-synthesized, partially evacuated and fully evacuated α-$Mg_3(HCOO)_6$, and e) SEM of fully evacuated α-$Mg_3(HCOO)_6$.

the phase transition from α-$Mg_3[HCOO]_6$ to β-$Mg[HCOO]_2$.[19] Above 520 °C, β-$Mg[HCOO]_2$ decomposes to MgO. The amount of DMF calculated from TGA in as-synthesized MOF is 18.5 wt% compared to 6.5 wt% after partial evacuation. Furthermore, the morphology of the fully-evacuated α-$Mg_3[HCOO]_6$ has been investigated by SEM as depicted in Figure 1e. The monoclinic structure of α-$Mg_3[HCOO]_6$ is clearly shown in the SEM image with a crystal length between 5 to 20 μm. In this study, fully- and partially-evacuated α-$Mg_3[HCOO]_6$ MOFs were used to prepare semi-solid electrolytes (sSEs) in order to investigate the effect of guest solvents on the ionic conductivity. However, before it was important to exclude any contributions of other charge carriers, such as protons. Therefore, the EIS of the pure MOF solvated in tetraglyme (G4) was also measured (see the supporting information, Figure S1). The solvated MOF showed an unstable Nyquist plot with many scattered points after 24 h of cell assembly, indicating its insulating behavior and its high interfacial resistances. After 6 days of cell assembly, the cell stabilized due to the stabilization of the interfacial resistance and showed a semi-circle in the MΩ range, and its calculated ionic conductivity is found to be 5.1×10^{-10} S cm^{-1}. This residual ionic conductivity is attributed to charge-balancing defect sites within the framework[19] or corresponds to its proton conductivity. Due to the low ionic conductivity of α-$Mg_3[HCOO]_6$, it is well-suited to be used as a matrix for Mg salts. However, an appropriate solvent is necessary for the Mg salts in order to allow dissolution of Mg^{2+} ions into the cavities of α-$Mg_3[HCOO]_6$. Of course, even some of the solvent molecules themselves fill the cavities of MOFs as free molecules or solvated Mg^{2+} ions, depending on the solvation properties of each solvent. Therefore, the effect of Mg salt constituents and composition as well as the guest solvent on the ionic conductivities of MOFsSEs has been investigated systematically.

First, the effect of Mg salts on the ionic conductivity was investigated. Therefore, $MgClO_4$, $MgBH_4$ or $Mg[TFSI]_2$-$MgCl_2$ (1:1 wt%) was added to the α-$Mg_3[HCOO]_6$ using G4 as a guest solvent. Thus, after evaporating the excess solvent, three different free standing sSEs were obtained, which depending on the added Mg-salt were named *p*MOFsSE-ClO_4, *p*MOFsSE-BH_4, and *p*MOFsSE-TFSI/Cl_2. The ionic conductivities of the resulting MOFsSEs were measured at 30 °C as mentioned in the experimental section. As shown in Figure S2, the Nyquist plots show only one semi-circle in the high-frequency region indicating that the ionic conductivity is related to the bulk of the material. The ionic conductivities were measured from the resistance value at the right-hand minimum of the semicircle as previously reported.[12] *p*MOFsSE-TFSI/Cl_2 affords the highest ionic conductivity of 1.24×10^{-5} S cm^{-1} compared to 7.87×10^{-7} S cm^{-1} for *p*MOFsSE-ClO_4. While *p*MOFsSE-BH_4 revealed the lowest ionic conductivity of 2.30×10^{-8} S cm^{-1} that could be due to the poor solvation of magnesium borohydride in G4. Moreover, $Mg[TFSI]_2$ has a low ability to form aggregates during the solvation process due to the bulky size of $TFSI^-$ and highly-delocalized charges within it resulting in a better dissociation

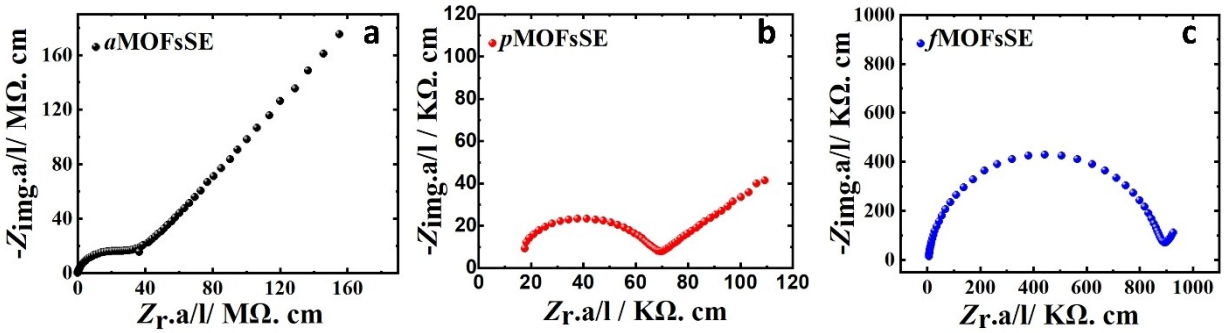

Figure 2. Nyquist plots at 30 °C of a) SS/*a*MOFsSEs/SS, b) SS/*p*MOFsSEs/SS and c) SS/*f*MOFsSEs/SS. Tetraglyme (G4) and 10 wt% $Mg[TFSI]_2$-$MgCl_2$ (1 : 1 wt. ratio) were used for MOF solvation as guest solvent and as source for Mg ions, respectively.

compared to *p*MOFsSE-ClO_4 that has a high tendency to form ion pairs and aggregates.[21]

Based on the results mentioned above, the mixture of $Mg[TFSI]_2$-$MgCl_2$ (1 : 1 wt%) has been selected for further studies. Herein, the effect of MOF evacuation on the ionic conductivities of MOFsSEs and their corresponding electrochemical performance in the presence of Mg electrodes has been investigated by electrochemical impedance spectroscopy (EIS), cycling voltammetry (CV) and galvanostatic measurements. The α-$Mg_3[HCOO]_6$ MOF has been synthesized as described in the experimental section and used as a matrix for MOFsSEs either directly or after partial or full evacuation. The resulting MOFs were mixed with 10 wt% $Mg[TFSI]_2$-$MgCl_2$ (1 : 1 wt%) and solvated in G4, followed by evaporation of the solvent that results in free-standing MOFsSEs. The ionic conductivities of these three MOFsSEs were then evaluated by EIS measurements. The corresponding Nyquist plots depicted in Figure 2a, b and c show that MOFsSEs prepared directly after MOF synthesis without evacuation results in very high ionic resistances compared to what was obtained if the MOFs had been evacuated first. Surprisingly, the MOFsSE prepared from the fully evacuated MOF (*f*MOFsSE) showed a higher ionic resistance compared to what was obtained from the partially evacuated one (*p*MOFsSE). The ionic conductivity of *f*MOFsSE at 30 °C is calculated as 1.1×10^{-6} S cm^{-1} compared to 1.4×10^{-5} S cm^{-1} and 0.2×10^{-7} S cm^{-1} for *p*MOFsSE and as-synthesized *a*MOFsSE, respectively. The remaining DMF in the partially evacuated MOF plays an additional role in the solvation of Mg salts, leading to a different solvation structure compared to what is obtained in G4. The low ionic conductivity obtained with *a*MOFsSE is attributed to the low probability of solvated salts to fill the pores of MOFs that are already fully filled with DMF molecules.

To investigate the effect of DMF content on the Mg electrode, symmetric Mg/Mg cells have been assembled for the three MOFsSEs with a different DMF content (*a*MOFsSEs, *p*MOFsSEs, and *f*MOFsSEs). The EIS and galvanostatic measurements of these three symmetric Mg/Mg cells are depicted in Figure 3. Due to the different structure obtained in glyme as solvent compared to that obtained in different DMF/glyme mixtures, their corresponding EIS at open circuit voltage (OCV) are different. *a*MOFsSE showed more capacitive nature compared to the others as indicated by the increased angle (close to 90°) of the spike in the low frequency region compared to the others due to low probability of solvated salts to fill the pores of MOFs that are already fully filled with DMF molecules before *a*MOFsSE preparation as have been previously mentioned. This implies a dominant capacitive behavior and restricted ionic diffusion in MOFsSE prepared from the as-synthesized MOF compared to the others that showed a more resistive behavior and better ionic diffusion.

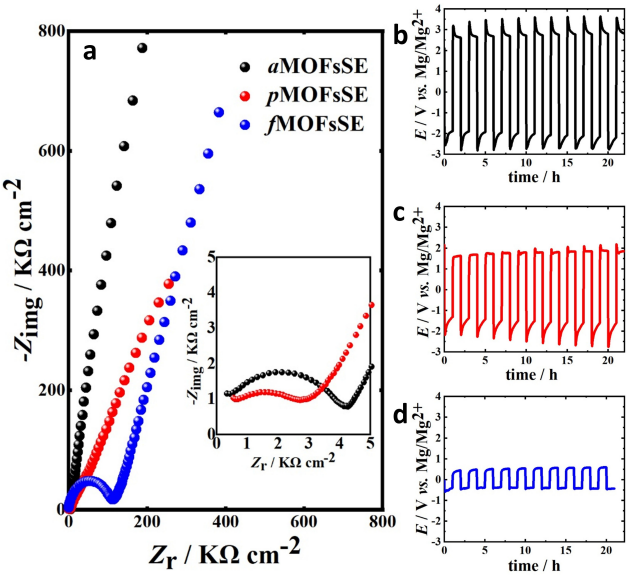

Figure 3. a) Nyquist plots of symmetric Mg/Mg cells of *a*MOFsSE, *p*MOFsSE and *f*MOFsSE, and b), c) and d) The corresponding galvanostatic measurements at 0.1 μA cm^{-2} respectively where, DME was used as guest solvent and 20 wt% $Mg(TFSI)_2$-$MgCl_2$ (1 : 1 wt. ratio) were used as source of Mg ions. The measurements have been conducted at 40 °C.

On the other hand, as obtained by the galvanostatic measurements, the *f*MOFsSE provided the best performance in the presence of Mg electrodes compared to the others, while the largest Mg deposition/stripping overpotential was obtained from *a*MOFsSE.

The change in the galvanostatic cycling shape indicates that the presence of DMF in MOFsSEs results in difficulties in the Mg deposition/stripping processes due to the interaction with Mg electrodes that leads to a change in galvanostatic curves

despite the relatively higher ionic conductivity obtained from *p*MOFsSE. Additionally, both *a*MOFsSE and *p*MOFsSE contain DMF besides the glyme solvent added to solvate Mg salts. Therefore, they contain DMF/glyme mixtures instead of only glyme (the case of *f*MOFsSE) that results in a change in the solvated Mg ion structure and, consequently, different electrochemical performance.

Several reports investigated the effect of the addition of DMF to the polymer-based Li electrolytes that seems to provide very high Li^+-conductivity.[22–30] However, some other reports showed that the addition of DMF must be handled with a certain care due to the reduction of DMF by Li metal that affects the interface with Li metal. Zhu et al.[22] showed that the addition of 8.6 wt% DMF to the polymer electrolyte afford a very high ionic conductivity at room temperature of 0.1 mS cm^{-1} However, it showed severe continuous interaction with Li metal and the cell fails in only several hours. Therefore, the presence of DMF may enhance the ionic conductivity several order of magnitude but it affects the interface with metal electrode that leads to side reactions. Therefore, the (pseudo) high ionic conductivity of DMF containing electrolytes is not necessary resulting in better electrochemical performance during cycling with Mg electrodes.

These differences in the ionic conductivity values and electrochemical performance of the partially evacuated MOF compared to those of the fully evacuated MOF has inspired us to further investigate the effect of the guest solvent. Therefore, in this work, fully evacuated MOF was used for further investigations to avoid misleading results that might arise from the presence of DMF traces in the structure.

Initially, the loading of Mg salts was optimized, after which the effect of guest solvent was investigated. Three different compositions of Mg salts (10, 20, and 30 wt%) were added to the fully-evacuated MOF in the presence of G4 solvent. Finally, the ionic conductivities of the three obtained MOFsSEs were measured at 100 °C. As shown in Figure S3, increasing the Mg salt to 20 wt% results in an increase in the ionic conductivity value. Increasing the salt composition to 30 wt% did not show a significant effect on the ionic conductivity value compared to 20 wt%, rather a slight decrease in ionic conductivity was observed, which in principle does not represent a big difference (45 μS cm^{-1} compared to 55 μS cm^{-1} for 30 wt% and 20 wt%, respectively). This slight decrease indicates the saturation of the MOF due to the filling of all its pores. These results indicate that 20 wt% of total Mg salt seems to be the optimal mass loading.

Noteworthy, the coordination between the magnesium ions and the anion causes anion decomposition and/or impedes the magnesium deposition process. Therefore, the separation of the anion from the magnesium ion is crucial to accelerate magnesium deposition,[31] which seems to be the main role of MOF and its guest solvent.

Because solvent molecules play an important role in determining the association of the ions into ion pairs, complexes, aggregates, or even free ions, they might have a tremendous impact on the resulting ionic conductivities. Therefore, solvents of different nature and solvation strength, such as monoglyme (dimethoxyethane, DME), G4, diethylene glycol (DEG), acetone, and DMF, have been used to solvate Mg ions and MOF. DMF, DEG, and acetone were included in this study because they are commonly used solvents to handle MOFs. While DMF is the most frequently used solvent to synthesize MOF by the hydrothermal reaction, DEG has also been used as a solvent to synthesize MOFs as well as as plasticizer, while acetone is used for solvent exchange for MOFs with low thermal stability and high risk of structural collapse during solvent evacuation. This will provide more fundamental insights into the importance of careful handling of MOFs and the mandatory removal of the remaining guest solvent prior to their use in battery applications. Figure 4a shows the Nyquist plots of *f*MOFsSEs prepared in these various solvents at 50 °C. It is observed that *f*MOFsSEs-DME provided the highest ionic conductivity compared to the others. This could be due to the simpler complex formed between Mg^{2+} ions and DME compared to the extended structure of G4 that reduces ion mobility. Variations in ionic conductivities with temperature have been investigated in the temperature range between 30 and 100 °C and the corresponding Nyquist plots are shown in Figure S4. Surprisingly, *f*MOFsSE-DMF revealed higher ionic conductivities at temperatures above 50 °C. As shown in Figure 4b, the increase in ionic conductivities of *f*MOFsSEs prepared in different solvents obeys the Arrhenius relation. The activation energy for diffusion E_a was calculated from the slope of the Arrhenius plot. The comparison between the activation energy of diffusion (E_a) and the conductivity values achieved at 50 °C for the *f*MOFsSEs with different guest solvents is shown in Figure 4c. It is visible that the ethereal solvents provide the lowest E_a compared to the other solvents. To reveal whether this ionic conductivity trend is related to the content or the nature of the guest solvent, TGA analyses were performed for all *f*MOFsSEs (Figure S5). The solvent content in each *f*MOFsSE has been calculated from the mass loss as follows: 20.9 wt% in *f*MOFsSEs-G4, 28 wt% in *f*MOFsSEs-DMF, 17.8 wt% in *f*MOFsSEs-acetone, 27 wt% in MOFsSEs-DEG, and 15.7 wt% in *f*MOFsSEs-DME. Consequently, *f*MOFsSEs-DMF and *f*MOFsSEs-DEG showed the highest solvent content compared to those of the other *f*MOFsSEs, indicating that the change in ionic conductivity is directly related to the nature of the guest solvent more than to their content.

Since the behavior of the Mg ions inside the MOFs cavities is not clear, and the role of the guest solvents after *f*MOFsSE preparation is also not fully understood, we tried understanding the obtained ionic conductivity values on the basis of the solvation properties of the guest solvents. Meanwhile, the solvation strength of a solvent can play an important role in the ionic conductivity of magnesium electrolytes. The ability of a solvent to solvate the organic magnesium salt can impact its dissociation into magnesium ions and the organic anions. Polarity, dielectric constants, Lewis basicity, the tendency to form ion pairs, and stability of the complex formed with Mg ions are all factors that could affect the ionic conductivity of an electrolyte.[32,33] *f*MOFsSE-acetone showed the lowest ionic conductivity due to the low Lewis basicity of acetone compared to the other solvents.[34,35] Among the solvents mentioned, DMF and DEG are known to strongly coordinate with Mg ions. DMF

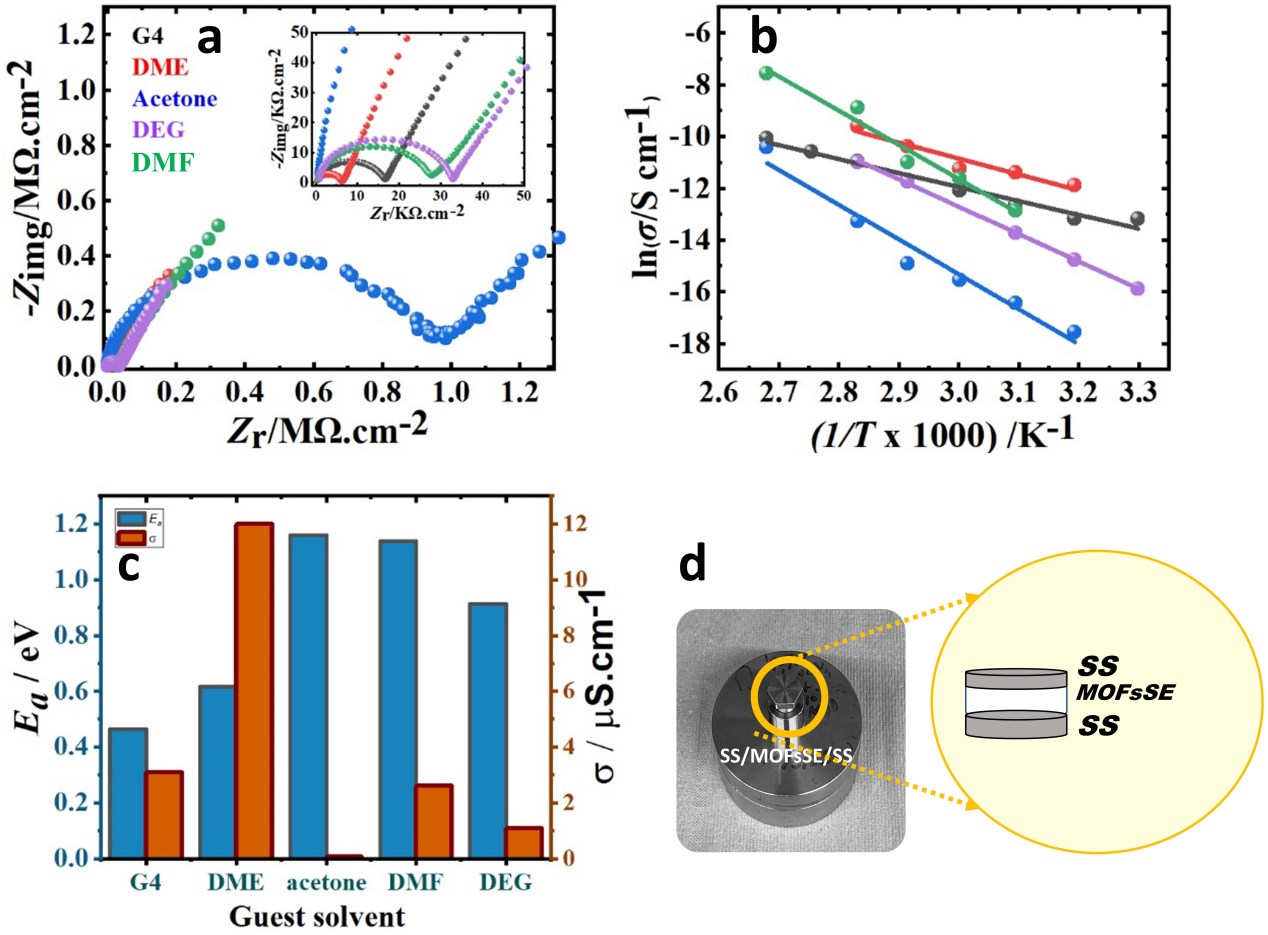

Figure 4. a) Nyquist plots of MOFsSEs prepared in different guest solvents at 50 °C, b) The corresponding Arrhenius plot, c) calculated ionic conductivities at 500 °C and the corresponding E_a, and d) cell used for EIS measurements.

has a high dielectric constant and a high Lewis basicity, which makes it an excellent solvent for coordinating with Mg ions. Diethylene glycol also has a high dielectric constant and good coordinating ability, but to a lesser extent than DMF. Moreover, due to the high polarity of DMF and DEG solvents,[34] their ability to solvate $Mg[TFSI]_2$ plays a crucial role in the observed high ionic conductivity at temperatures above 50 °C at which the complex becomes weaker and therefore allows Mg ion diffusion. Meanwhile, glyme-based solvents, such as monoglyme and tetraglyme, have a unique ability to solvate Mg ions and form stable solvated complexes, which can enhance the electrochemical performance of Mg-ion batteries. Compared to other solvents, such as DMF and DEG, monoglyme and tetraglyme have been widely used in Mg ion batteries[32,36–38] due to their high affinity to solvate Mg ions and to form not too stable complexes, which can lead to slow kinetics and poor Mg electrodeposition.

The relatively high ionic conductivity of *f*MOFsSE-DMF especially at relatively high temperatures inspired us to further investigate the effect of DMF in more details. Therefore, symmetric Mg/Mg cell with *f*MOFsSE-DMF electrolyte has been assembled and characterized by CV, galvanostatic measurements and SEM/EDX with elemental mapping as shown in Figure 5. Cyclic voltammogram of Mg/*f*MOFsSE-DMF/Mg revealed in Figure 5a showed a significant drop in the peak current after the first cycle and the cell impedance increased significantly after CVs (Figure 5b) that indicates side reactions took place on the electrode surface due to a possible electrolyte decomposition resulting in an electrode passivation. The first trial to do galvanostatic measurements using the same potential window as in CVs showed inability to deposit Mg from *f*MOFsSE-DMF as shown in Figure 5c. Upon increasing the reduction potential limits to −3 V, the galvanostatic measurements (Figure 5d) showed reduction plateau at nearly −2.0 V that increased to −2.3 V upon cycling and the corresponding oxidation at 2.1 V that increased to 2.3 V upon cycling. This huge overpotential of Mg/*f*MOFsSE-DMF/Mg at relatively low current (0.1 μA) could be attributed to the presence of free DMF molecules that i) have high affinity to be adsorbed on the Mg electrode and block the active sites, ii) DMF is not sufficiently stable towards the Mg surface and undergoes decomposition during the anodic scan that leads to passivation of the Mg electrode by decomposition products and hinders the Mg deposition/stripping reaction, and iii) DMF catalyzes the formation of surface metal oxides and consequently passivates the Mg electrode.[29]

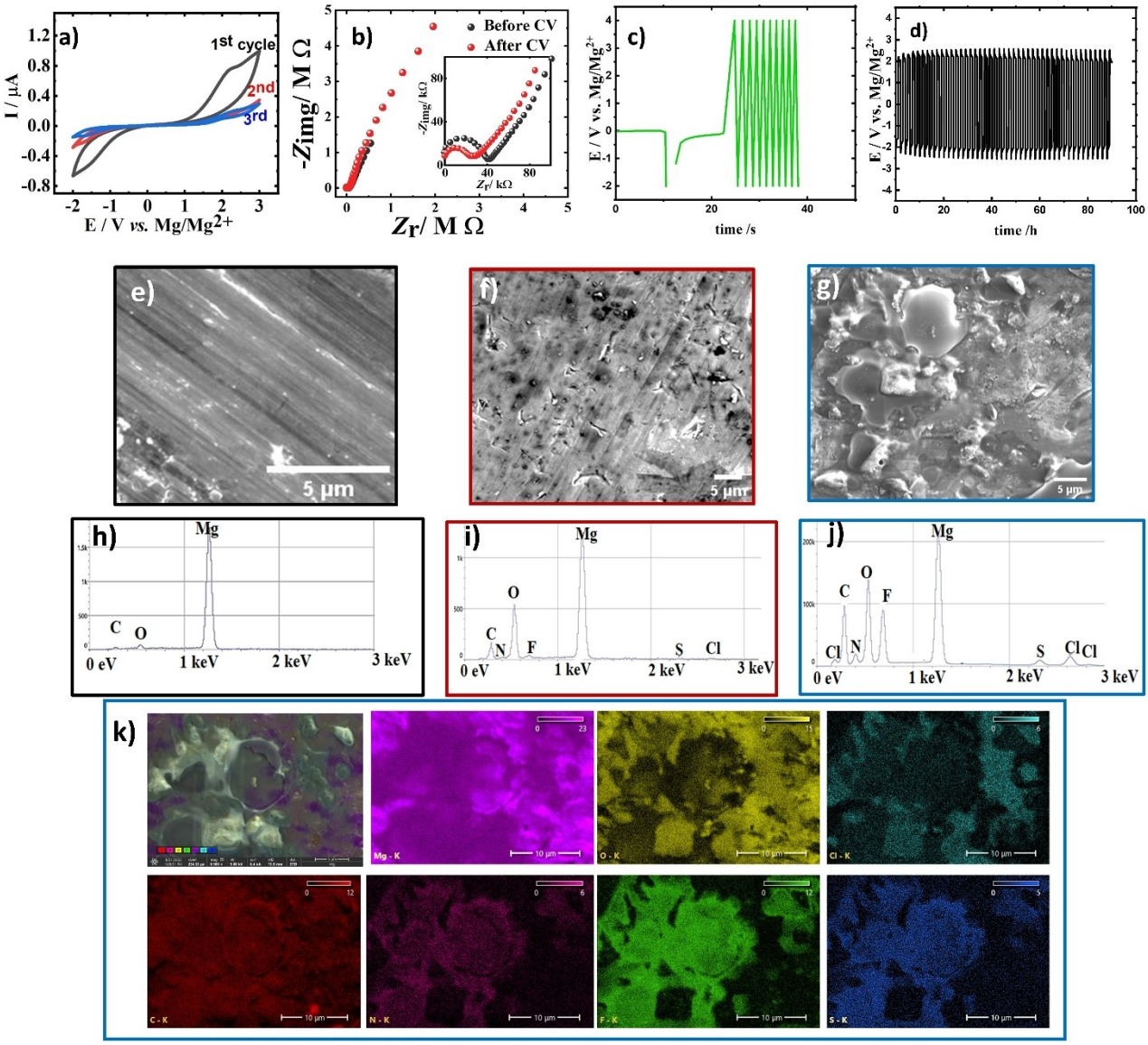

Figure 5. a) CV of Mg/*f*MOFsSE-DMF/Mg measured at 40 °C at scan rate 0.5 mV s^{-1}, b) The corresponding Nyquist plot before and after CVs, c) Galvanostatic measurement at ±0.1 μA, d) Galvanostatic measurement at ±0.1 μA with extended potential limits, e) SEM image of Mg electrodes before cycling, f) SEM image of Mg counter electrode after galvanostatic cycling, g) SEM of Mg working electrode after galvanostatic cycling, h), i) and j) corresponding EDX, respectively, and k) The corresponding elemental mapping of Mg working electrode.

In order to support this assumption, Mg electrodes were characterized by SEM/EDX and elemental mapping before and after galvanostatic measurements as shown in Figure 5 e–k. As clearly shown both Mg counter and working electrodes showed an increase in oxygen that support the third assumption mentioned above as well as SEM of working electrode showed the presence of decomposed products mainly from $TFSI^-$ anion and DMF as indicated from the elemental mapping shown in Figure 5k which supports the second assumption.

Based on the results summarized above, the remaining DMF in the MOF may lead to (pseudo) high ionic conductivity values; however, its presence leads to the passivation of Mg electrodes as summarized in Scheme 1. This should be taken into account when utilizing MOFs in Mg batteries.

Further, the electrochemical performance of *f*MOFsSE-G4 in the presence of Mg electrodes compared to *f*MOFsSE-DME was investigated by EIS, CV, and galvanostatic measurements as shown in Figure S6.

The CVs in Figure S6b shows that the *f*MOFsSE-G4 showed less Mg deposition/stripping abilities compared to *f*MOFsSE-DME. Meanwhile, *f*MOFsSE-G4 showed significantly lower Mg deposition/stripping currents compared to *f*MOFsSE-DME, indicating slower kinetics of Mg^{2+} ions in *f*MOFsSE-G4. This could be attributed to the simpler structure of the Mg/DME complex, especially inside the cavities of the MOF, the low viscosity of DME compared to G4, as well as the increased donor number of DME (24.0 kcal/mol) compared to G4 (16.6 kcal/mol).[30]

The Mg dissolution in MOFsSE-DME showed two steps of dissolution in the first cycle, as indicated by the appearance of

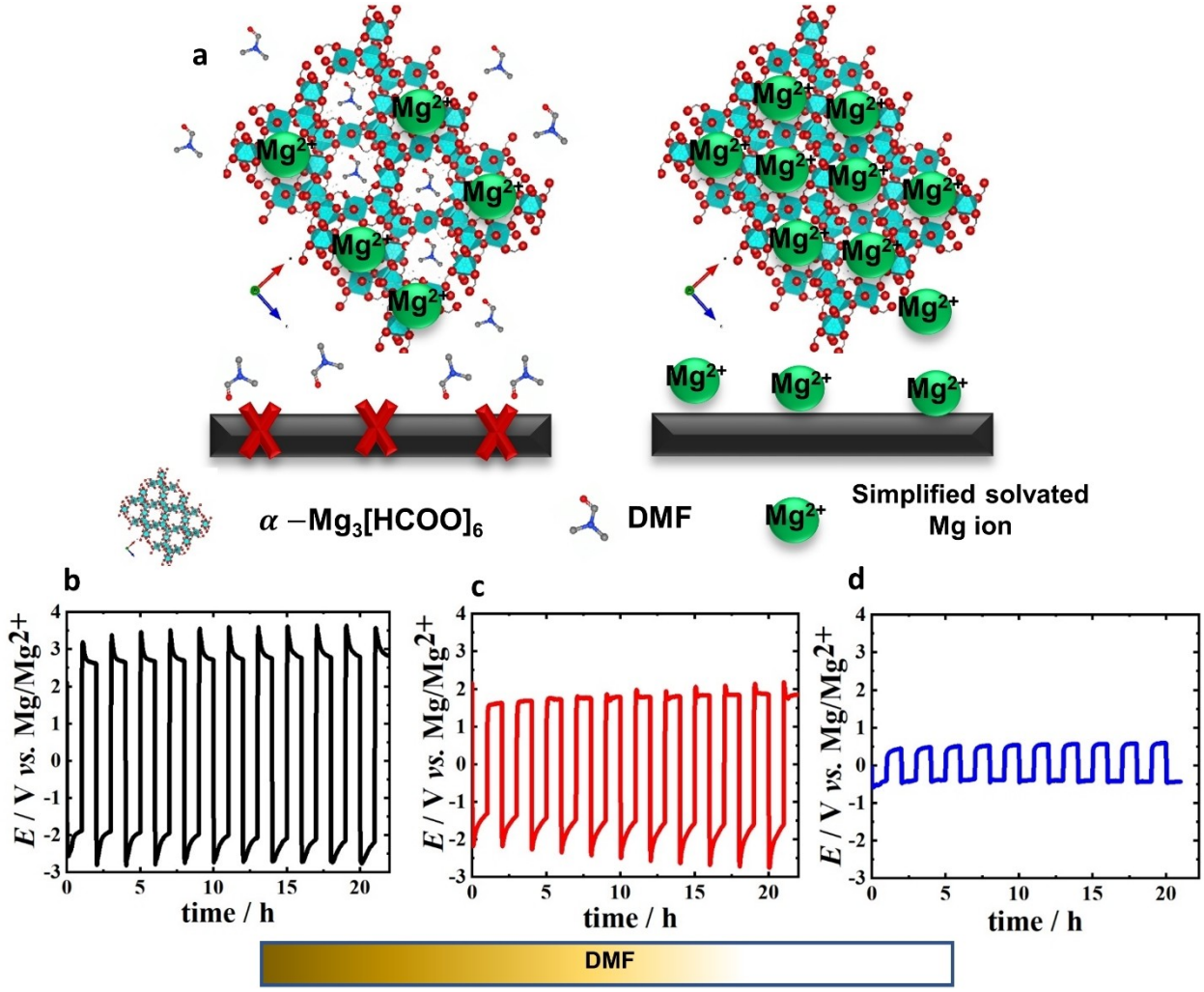

Scheme 1. a) Schematic figure shows the effect of the DMF on the passivation of the Mg electrode and consequently on the overpotential of Mg deposition and stripping reactions, b) The galvanostatic measurement of Mg/Mg cell obtained when MOF was used directly after synthesis and glyme solvent was added to solvate Mg^{2+} (*a*MOFsSE), (c) The galvanostatic measurement of Mg/Mg cell when the MOF was partially evacuated and glyme solvent was used for Mg^{2+} solvation (*p*MOFsSE), and d) The galvanostatic measurement of Mg/Mg cell when all DMF molecules were removed from the structure (*f*MOFsSE) that showed a significant enhancement in the Mg deposition/stripping overpotential.

two dissolution peaks at 1.5 and 1.9 V, while those peaks were combined into one peak in the subsequent cycles, as will be discussed later.

The galvanostatic measurements of Mg/*f*MOFsSE-G4/ Mg (Figure S6c) showed a higher potential barrier for Mg deposition from *f*MOFsSE-G4 compared to *f*MOFsSE-DME (see Figure 3d) with Mg deposition and dissolution potentials at −1.0 and 1.5 V, respectively, in the first cycle that increased to −1.8 and 2.0 V in subsequent cycles, respectively. These values are significantly higher than those observed by *f*MOFsSE-DME that showed Mg deposition and dissolution at −1.5 V and 0.5 V, respectively.

Due to the results obtained so far, *f*MOFsSE-DME was selected for our further structural and electrochemical investigations.

Characterization of MOFsSE-DME

The morphology of *f*MOFsSE-DME was investigated by SEM/EDX. As depicted in Figure 6a, the crystals are slightly deformed and covered with filament-like material, which is more likely due to absorption of solvent molecules. The solvated Mg ions also form homogeneous networks on the surface of the MOF crystals. The corresponding EDX spectrum shown in Figure 6b contains chloride, sulfur, and fluoride coming from both $MgCl_2$ and $Mg[TFSI]_2$. Furthermore, the amount of carbon increased compared to pure MOF, which is due to the added solvent and $Mg[TFSI]_2$. The small aluminum peak observed is from the sample holder. Meanwhile, the XRD of *f*MOFsSE-DME shown in Figure 6c does not show a significant change in the crystallinity of α-$Mg_3[HCOO]_6$ after *f*MOFsSE-DME preparation, indicating that the frameworks retain their integrity while being filled with solvated Mg ions and free solvent molecules. The shift in the peak positions to a lower angles reflects the increase in the

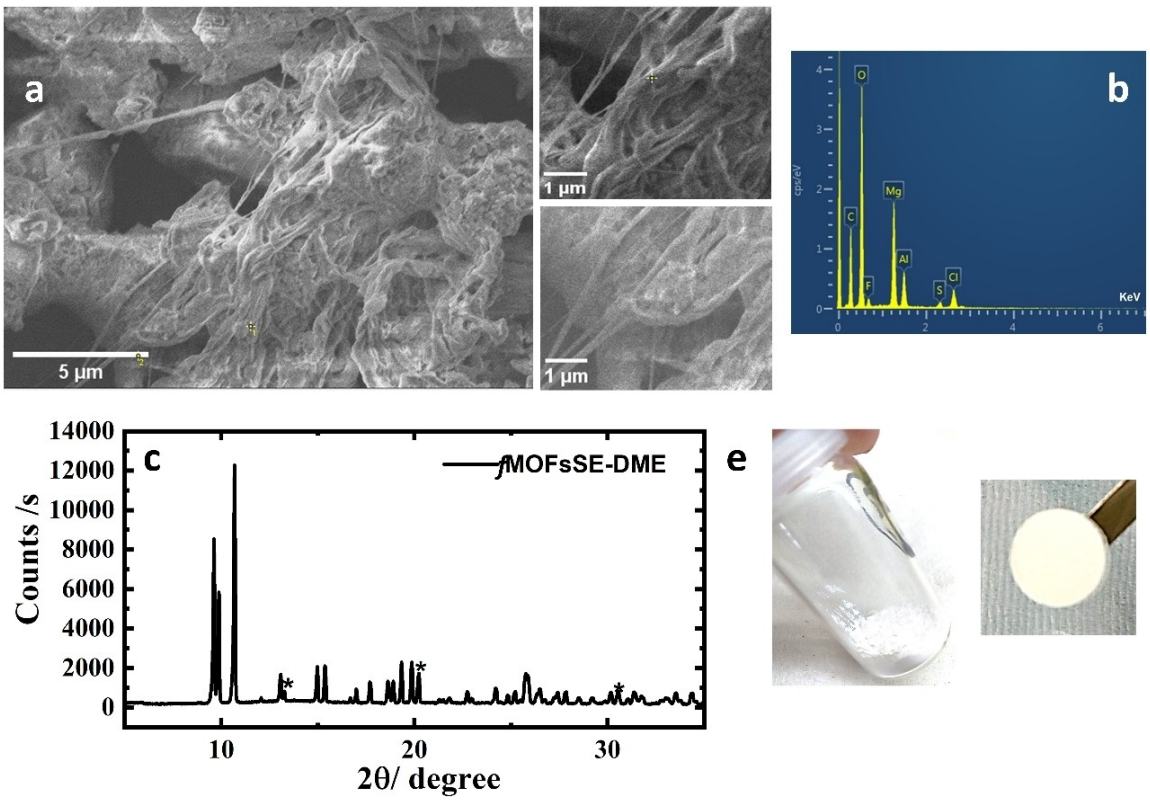

Figure 6. a) SEM image of *f*MOFsSE-DME at EHT = 3.00 kV with different magnifications, b) The corresponding EDX, c) The corresponding PXRD; the star shapes refer to $MgCl_2$ diffractions, and d) The resulting MOFsSE pellet after solvent evaporation and its pellet after pressing at 5 tones for 3 minutes.

crystal lattice due to the electrolyte uptake. These observations refer to the fact that some of the solvated Mg ions are also adsorbed on the surface of the crystals, forming the network shape, not only embedded into their cavities. To investigate the usability of *f*MOFsSE-DME for magnesium-ion batteries, the total transport number, the transference number, the cycling stability, and its behavior during charge and discharge at different current densities were examined.

The total transport number calculated by DC polarization of *f*MOFsSE-DME between two SS ion-blocking electrodes at 0.5 V using Equation (3) was found to be 0.992, where I_0 and I_S were determined directly from the *I vs. t* curves as shown in Figure S7. This indicates that the total current is mainly due to the ion motion with sluggish contribution from the electrons. Another important physical quantity of electrolytes is the cations transference number (t_+) that provides information about the quantity of the charged species inside the electrolyte, which is responsible for the charge transport. t_+ was calculated by the Vincent and Bruce equation (Eq. (4)). Chronoamperometry (*CA)* was used to measure I_0 and I_S and the EIS measurements before and after the *CA* to obtain R_0 and R_S (see. Figure 7a). The calculated value of the transference number was found to be $t_+ = 0.466$. That means that 46.6% of the transported charge of the electrolyte is carried by cations. This value is significantly improved compared to what was previously mentioned in literature for polymer-based sSEs,[40] while there is no reported t_+-value for MOF-based sSEs, except in our previous study.[16] Galvanostatic measurements were carried out at different current densities, and showed a reversible Mg deposition/stripping process as shown in Figure S8a. As a result of the relatively low ionic conductivity of MOFsSE-DME at the measurement temperature compared to the liquid analogue, relatively low current densities were used in this study. No significant change in the deposition and stripping potentials was observed after cycling. However, a small shift in the dissolution and deposition potentials at higher current densities was observed, preserving good cycling stability. The EIS after galvanostatic cycling (Figure S8b) showed a lower resistance compared to the initially recorded one, indicating improved kinetics after cycling.

On the other hand, the cycling stability of *f*MOFsSE-DME was also investigated by CV for a symmetric Mg/*f*MOFsSE-DME/Mg cell (Figure 7b). As previously mentioned, the first CV of the Mg/*f*MOFsSE-DME/Mg cell showed a Mg deposition at −1.5 V *vs.* Mg^{2+}/Mg with an onset potential of −0.47 V and two dissolution steps at 1.5 and 1.9 V. The deposition and dissolution currents significantly decreased on the second and third cycles, then stabilized but with an increase in the overpotentials upon cycling, which is consistent with galvanostatic results. Surprisingly, when galvanostatic measurements were conducted after CV cycling under these reaction conditions, an improved overpotential was obtained compared to the initial measurements referring to a conditioning process as shown in Figure 7c. The Mg deposition and dissolution

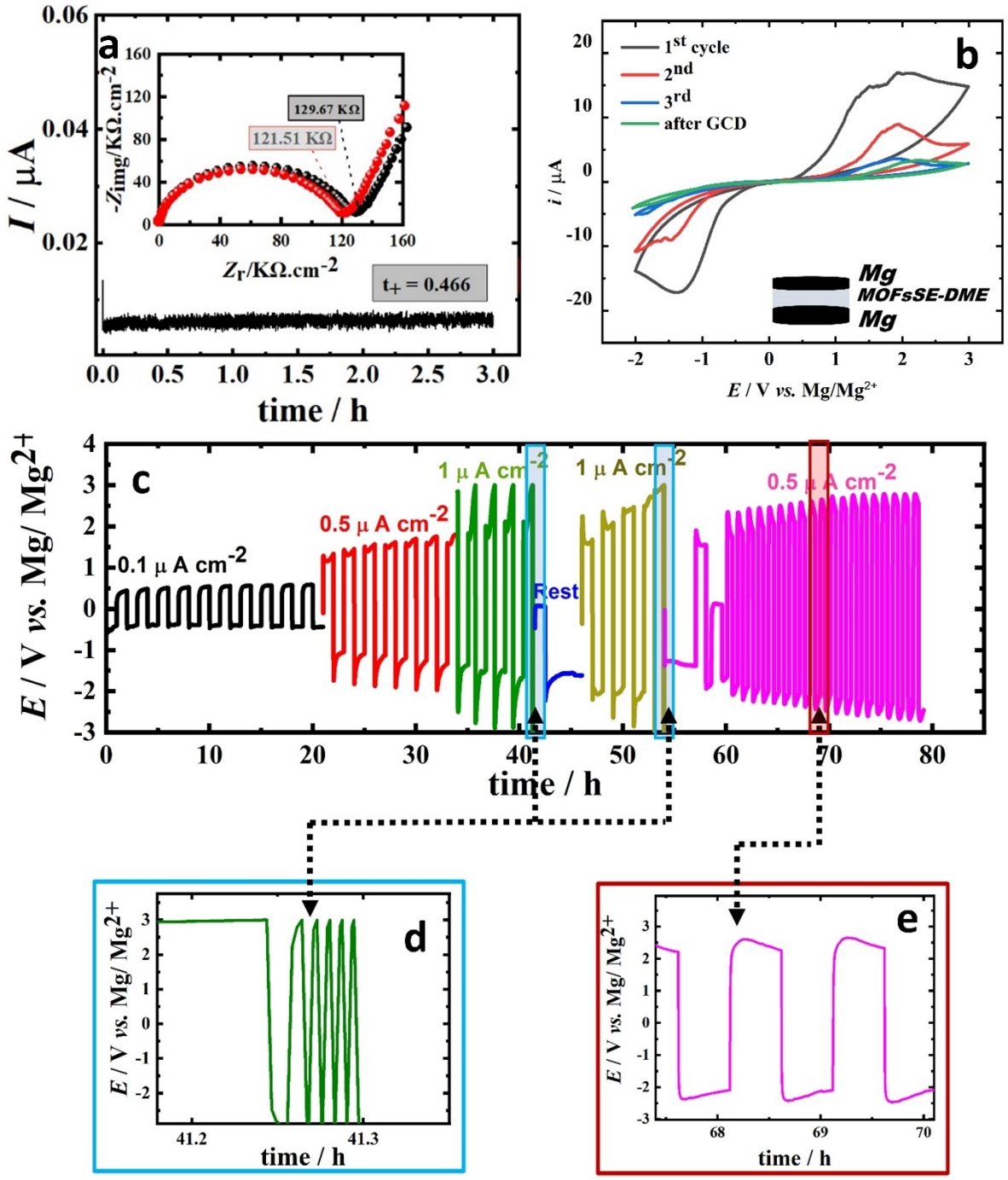

Figure 7. a) Polarization of Mg/*f*MOFsSE-DME/Mg at 30 mV for 3 h (Inset: The Nyquist plot before and after polarization, b) Repeated CVs of Mg/*f*MOFsSE-DME/Mg at 0.5 mV s^{-1} before and after galvanostatic cycling, c) Galvanostatic cycling of Mg/*f*MOFsSE-DME/Mg at different current densities, d) A zoom in to show the cycling fading observed at 1.0 μA cm^{-2}, and e) a zoom in to show the overpotential observed at 0.5 μA cm^{-2}. All measurements have been conducted at 40 °C.

processes were observed at −0.5 and 0.5 V, respectively. However, when increasing the current density to 1.0 μA cm^{-2}, the cell showed a very high overpotential, while Mg deposition occurred at −1.8 V and dissolution at 1.58 V (*vs.* Mg^{2+}/Mg).

The overpotential continues to increase upon cycling until complete fading as an indication of the low stability at this current density or due to blocking the Mg anode. However, when the cell was left to rest at OCV for several hours, Mg deposition/stripping could be re-observed for a few cycles after which it faded again. When the current density was reduced to 0.5 μA cm^{-2}, the deposition/stripping reactions showed up again, while the overpotential increased upon cycling, indicating that the cell was still working, although *f*MOFsSE-DME is highly-sensitive to current densities. This low tolerance to the

relatively high current densities could be due to the low ionic conductivity of *f*MOFsSE-DME at the measurement temperature. Compared to our previous work on mixed MOF (crystalline α-$Mg_3[HCOO]_6$ and amorphous Mgbpdc),[16] α-$Mg_3[HCOO]_6$-based sSEs showed lower stability at relatively high current densities. This indicates the significance of the MOF structure in designing an efficient MOFsSE. Therefore, designing a MOF with specific properties that enables a reversible Mg deposition and stripping at relatively high current densities is highly desired. This might open the door to designing new MOFs with specific functionalities and to investigate additives that can boost the performance of MOFsSEs.

On the other hand, the *f*MOFsSE-DMF showed very high stability over time, where the symmetric Mg cell has been left for few months after the measurement then measured one more time at different current densities as shown in Figure S9. This shows that cell aging does not significantly affect the ability of *f*MOFsSE-DME to deposit Mg, indicating the high stability of the electrolyte in contact with the Mg electrodes.

Furthermore, the ability to deposit Mg from *f*MOFsSE-DME on Cu has been also investigated by CV using Cu as working electrode as shown in Figure S10. A Mg deposition peak is observed at −1.2 V and the corresponding dissolution at 2.8 V. Meanwhile, the SEM/EDX of both counter and working electrode showed no decomposed products after cycling.

Conclusions

Based on the current study, one can conclude that selecting the appropriate guest solvent in MOF-based electrolytes is crucial for developing new electrolytes for Mg-ion batteries. Full evacuation of the MOF before its use in rechargeable Mg batteries as one of its components (electrolyte or electrode material) is crucial to realize a reversible deposition/stripping process and to prevent Mg passivation by the remaining DMF molecules. The presence of DMF in the sSEs leads to (pseudo) high ionic conductivity, however did not result in better electrochemical performance during cycling with Mg electrodes. The ex-situ SEM/EDX of MOFsSE-DMF showed the presence of high oxygen percentage on both counter and working electrode surfaces and decomposed products mainly from $TFSI^-$ anion and DMF on the surface of Mg working electrode.

Furthermore, Mg deposition from MOFsSE-glyme showed better performance considering the preference of *f*MOFsSE-DME over MOFsSE-G4. It is noteworthy that in MOF-based sSEs, magnesium ions compete with the solvent molecules and the MOF to interact with the anions, which may lead to Mg ions interacting differently with the anions and solvent molecules in the presence of MOFs, finally leading to different coordination compounds.

It is worth mentioning that, the results shown in this study, especially the galvanostatic measurements, are limited to the components of the electrolyte that might alter when changing one or more of these components. Designing new MOFs with specific properties that enable the free movement of Mg^{2+} ions is crucial and might change the results of galvanostatic measurements.

In the future, further investigations of MOF-based electrolytes, through studying the solvation of Mg ions inside the MOF cavities and how these change in the presence and absence of MOF, will lead to a deeper understanding of MOF-based electrolytes that can help in their development. The role of MOF as one of the electrolyte components in a real battery with a high potential cathode material will also be studied individually.

Experimental Section

Materials and chemicals

Magnesium nitrate hexahydrate, formic acid, anhydrous *N,N*-dimethylformamide (DMF), dimethoxyethane (DME or G1), tetraglyme (G4), acetone, diethyleneglycol (DEG), magnesium(II) Bis(trifluoromethanesulfonyl)imide, ($Mg[TFSI]_2$), anhydrous magnesium chloride, $MgCl_2$, anhydrous magnesium perchlorate, $Mg(ClO_4)_2$, and magnesium borohydride, $Mg(BH_4)_2$ were purchased from Sigma Aldrich. All salts and powders were heated at 120 °C under a vacuum overnight and stored in an Ar-filled glovebox. All the solvents used for solid electrolytes preparation were further dried over 3 Å molecular sieves and stored in an Ar-filled glovebox. Mg foil (thickness = 0.025 mm, ⌀12 mm) was purchased from Alfa Aesar and has been used for the symmetric cell assembly.

Synthesis of α-$Mg_3[HCOO]_6$

α-$Mg_3[HCOO]_6$ has been prepared by the hydrothermal method in the presence of formic acid, where 3 mmol of Mg salt was mixed with 6 mmol of formic acid in 10 ml of DMF solvent followed by a hydrothermal reaction at 100 °C for 72 h. For partially evacuated MOF, as-synthesized material was heated under a vacuum of 10 mbar for 36 h at 130 °C. For the fully evacuated MOF, the as-synthesized material was heated under ultra-high vacuum (10^{-5} mbar) at 150 °C for 24 h. The activated MOFs were stored directly inside an Ar-filled glovebox with H_2O and O_2 levels less than 0.5 ppm for further use.

Preparation of MOF-based Mg semi-solid electrolytes (MOFsSE)

In an Ar-filled glovebox, sSEs were prepared by dispersing α-$Mg_3[HCOO]_6$ and Mg salts in different solvents, DME, G4, DEG, DMF, or acetone under continuous stirring for 48 h. Subsequently, the excess solvent was evaporated under vacuum and SEs were subjected to a vacuum drying at 80 °C (except for DME and acetone, samples were dried at 50 °C overnight under a vacuum of 40 mbar. This method has been used to minimize the solvent extent in MOFsSEs as mentioned in our previous work.[16] To investigate any ionic conductivities that may come from MOF, the solvated MOF was dispersed in G4 in the same way without the addition of Mg salts.

Surface, structural, and spectral characterization

Thermogravimetric analysis (TGA) data were collected with a TGA/SDTA 851e from Mettler Toledo in an N_2 atmosphere from room temperature to 600 or 800 °C with a heating rate of 5 °C/min. Powder diffraction X-ray (PXRD) was recorded on the STOE Stadi P

diffractometer under the following conditions: 40 kV, 40 mA, Cu-Kα radiation ($\lambda = 0.154$ nm) using the transmission mode. The semi-solid electrolyte powders were assembled in the sample holder and covered by acetate foil inside the glovebox to avoid air contamination. Xpert PANalytical Highscore software was used for PXRD pattern analysis. Scanning electron microscope images and energy dispersive X-ray spectroscopy were performed by Zeiss LEO 1550 VP field emission SEM/EDX (FESEM Carl Zeiss, Germany). A transfer box was used to transport samples from the glovebox to the SEM chamber without exposure to air. For nuclear magnetic resonance (NMR) analysis, the samples were digested in D_2O and sometimes heating was required for complete solubility. The ^{1}H-NMR spectra were recorded on NMR Bruker 400 MHz instruments, and the obtained spectra were analyzed by *MNOVA* software.

Electrochemical characterization

Electrochemical impedance spectroscopy (EIS) for the ionic conductivity measurements was recorded by the Solartron software. Cyclic voltammograms (CV), galvanostatic discharge-charging tests (GCD), and EIS between cycles were recorded by the biologic VMP3 multichannel potentiostat at 40 °C in a thermostatic climate chamber with a maximum deviation of ±1 °C unless otherwise noted. All the cells were left at OCV for 4 days before the measurements, which is the needed time to get a stable EIS. The sSE pellets were sandwiched between two Mg foils (thickness = 0.025 mm, ⌀12 mm, Alfa Aesar) for symmetric cell measurements.

For ionic conductivity measurements, in an Ar-filled glove box, 0.1 g of the sSE powder was dispensed between two stainless steel discs into a cylindrical homemade PEEK cell of an inner diameter of 13 mm. The loaded material was then pressed at 5 tons for three minutes prior to thickness measurements by a thickness gauge accurate to 0.2 μm. The thickness of the formed pellets is between 0.45 to 0.58 mm. Prior to the electrochemical tests, cells with the sSE pellets were housed in stainless steel cases with an upper screw applying a force to the upper part of the cell to ensure electrical contact and stable mechanical stability of the cells. The whole cell was further sealed in an aluminum case filled with Ar to avoid any possible exposure to air. *AC* impedance spectroscopy was used for conductivity measurements in a temperature range between 25 and 80 or 100 °C where the cells were kept at each temperature for two to three hours before measurement. All data was collected at 10 mV AC amplitude with a frequency range between 1 MHz to 100 or 1000 Hz, with 10 points per decade (except for solvated MOF, 100 mV AC amplitude was used). The solution resistances were determined from the right-hand minima of the high-frequency region of the Nyquist plots. Subsequently, the bulk conductivities were calculated by Equation (1):

$$\sigma = l/(R_s\ A) \tag{1}$$

Where σ is the bulk conductivity in S·cm^{-1}, l is the thickness of the pellet in cm, R_s is the solution resistance in Ohms and A is the area of the pellet area in cm^2. The pseudo-activation energies were calculated from the Arrhenius relation:

$$\sigma = \sigma_o \cdot e^{(-Ea/kBT)} \tag{2}$$

Where σ_0 is the pre-exponential factor, T is the absolute temperature in K, E_a is the pseudo-activation energy of diffusion and k_B is the Boltzmann constant.

For the calculation of the total transport number, SE pellets were sandwiched between two 13 mm diameter ion blocking stainless steel discs before applying a *DC* potential of 0.5 V for 3 or 4 hours until a steady-state current was achieved. Total ion transport was measured by Equation (3):

$$t_{ion} = (I_0 - I_s)/I_0 \tag{3}$$

Where, I_0 is the initial current (at $t = 0$), I_s is the steady-state current and t_{ion} is the total ion transport number. The Mg^{2+} ion transference number (t_+) was determined by coupling the *AC* EIS test with the DC polarization experiment, SE pellets were sandwiched between two ion non-blocking Mg foils. A small constant potential bias $\triangle V = 0.03$ V was applied, and the current was recorded vs. time until a steady-state current was obtained. EIS measurements were carried out before and after DC polarization, then t_+ is calculated from Bruce and Vincent Equation (4).[41]

$$i_+ = \frac{I_{s(\Delta V - R_0 I_0)}}{I_{0\ (\Delta V - R_s I_s)}} \tag{4}$$

Here, I_s and I_0 are steady state and initial currents, respectively, R_0 and R_s are the polarization resistances before and after the polarization, respectively and $\triangle V$ is the applied potential bias.

Data Availability

All data are available for sharing based on the DFG's Code of Conduct "Safeguarding Good Research Practice".

Acknowledgements

This work contributes to the research performed at CELEST (Center for Electrochemical Energy Storage Ulm-Karlsruhe) and we thank the German Research Foundation (DFG) for funding under Project ID 390874152 (POLiS Cluster of Excellence), and for funding within the priority program SPP 2248 Polymer-based Batteries (Project ID 441209207). Further, support by the BMBF (Bundesministerium fur Bildung und Forschung) through the project CASINO (FKZ: 03XP0487G) and the state of Baden-Württemberg and the DFG through grant no INST 40/574-1 FUGG is gratefully acknowledged. Open Access funding enabled and organized by Projekt DEAL.

Conflict of Interests

The authors declare no conflict of interest.

Data Availability Statement

The data that support the findings of this study are available from the corresponding author upon reasonable request.

Keywords: Mg batteries · metal-organic frameworks · semi-solid electrolytes · solvent effects · deposition

[1] P. W. Jaschin, Y. Gao, Y. Li, S.-H. Bo, *J. Mater. Chem. A* **2020**, *8*, 2875.

[2] R. Davidson, A. Verma, D. Santos, F. Hao, C. Fincher, S. Xiang, J. Van Buskirk, K. Xie, M. Pharr, P. P. Mukherjee, *ACS Energy Lett.* **2018**, *4*, 375.
[3] R. S. Kumar, M. Raja, M. A. Kulandainathan, A. M. Stephan, *RSC Adv.* **2014**, *4*, 26171.
[4] H. Chen, S.-Y. Han, R.-H. Liu, T.-F. Chen, K.-L. Bi, J.-B. Liang, Y.-H. Deng, C.-Q. Wan, *J. Power Sources* **2018**, *376*, 168.
[5] A. Rossin, M. R. Chierotti, G. Giambastiani, R. Gobetto, M. Peruzzini, *CrystEngComm* **2012**, *14*, 4454.
[6] A. Rossin, A. Ienco, F. Costantino, T. Montini, B. Di Credico, M. Caporali, L. Gonsalvi, P. Fornasiero, M. Peruzzini, *Cryst. Growth Des.* **2008**, *8*, 3302.
[7] E. D. Bloch, D. Britt, C. Lee, C. J. Doonan, F. J. Uribe-Romo, H. Furukawa, J. R. Long, O. M. Yaghi, *J. Am. Chem. Soc.* **2010**, *132*, 14382.
[8] M. L. Aubrey, R. Ameloot, B. M. Wiers, J. R. Long, *Energy Environ. Sci.* **2014**, *7*, 667.
[9] R. Zhao, Z. Liang, R. Zou, Q. Xu, *Joule* **2018**, *2*, 2235.
[10] S. S. Park, Y. Tulchinsky, M. Dinca, *J. Am. Chem. Soc.* **2017**, *139*, 13260.
[11] A. E. Baumann, D. A. Burns, B. Liu, V. S. Thoi, *Commun. Chem.* **2019**, *2*, 1.
[12] K. Pożyczka, M. Marzantowicz, J. R. Dygas, F. Krok, *Electrochim. Acta* **2017**, *227*, 127.
[13] E. M. Miner, S. S. Park, M. Dincaˇ, *J. Am. Chem. Soc.* **2019**, *141*, 4422.
[14] C. J. Barile, R. G. Nuzzo, A. A. Gewirth, *J. Phys. Chem. C* **2015**, *119*, 13524.
[15] J. Drews, P. Jankowski, J. Häcker, Z. Li, T. Danner, J. M. García Lastra, T. Vegge, N. Wagner, K. A. Friedrich, Z. Zhao-Karger, M. Fichtner, A. Latz, *ChemSusChem* **2021**, *14*, 4820.
[16] H. K. Hassan, A. Farkas, A. Varzi, T. Jacob, *Batteries & Supercaps* **2022**, 5, e202200260.
[17] H. Mao, J. Xu, Y. Hu, Y. Huang, Y. Song, *J. Mater. Chem. A* **2015**, *3*, 11976.
[18] J. A. Rood, B. C. Noll, K. W. Henderson, *Inorg. Chem.* **2006**, *45*, 5521.
[19] D. E. Kravchenko, A. J. Cruz, S. Rodríguez-Hermida, N. Wauteraerts, T. Hauffman, R. Ameloot, *Chem. Mater.* **2020**, *32*, 10469.
[20] J. Xu, V. V. Terskikh, Y. Chu, A. Zheng, Y. Huang, *Magn. Reson. Chem.* **2020**, *58*, 1082.
[21] N. N. Rajput, T. J. Seguin, B. M. Wood, X. Qu, K. A. Persson, *Elucidating Solvation Structures for Rational Design of Multivalent Electrolytes – A Review*. In: *Modeling Electrochemical Energy Storage at the Atomic Scale. Topics in Current Chemistry Collections* (Ed. M. Korth), Springer, **2018**.
[22] J. Zhu, S. He, H. Tian, Y. Hu, C. Xin, X. Xie, L. Zhang, J. Gao, S. Hao, W. Zhou, *Adv. Funct. Mater.* **2023**, *33*, 2301165.
[23] R. Baskaran, S. Selvasekarapandian, G. Hirankumar, M. S. Bhuvaneswari, *J. Power Sources* **2004**, *134*, 235.
[24] X. Zhang, T. Liu, S. Zhang, X. Huang, B. Xu, Y. Lin, B. Xu, L. Li, C.-W. Nan, Y. Shen, *J. Am. Chem. Soc.* **2017**, *139*, 13779.
[25] X. Zhang, S. Wang, C. Xue, C. Xin, Y. Lin, Y. Shen, L. Li, C. Nan, *Adv. Mater.* **2020**, *32*, 2000026.
[26] D. Callegari, S. Bonizzoni, V. Berbenni, E. Quartarone, P. Mustarelli, *Adv. Mater.* **2020**, *32*, 1907375.
[27] N. Senthilkumar, K. J. Babu, G. Gnana kumar, A. R. Kim, D. J. Yoo, *Ind. Eng. Chem. Res.* **2014**, *53*, 10347.
[28] A. R. Kim, K. S. Nahm, D. J. Yoo, R. Elizabeth, *J. Power Sources* **2010**, *195*, 5922.
[29] R. Hariprasad, M. Vinothkannan, A. R. Kim, D. J. Yoo, *J. Dispersion Sci. Technol.* **2020**, *42*, 33.
[30] M. Ranjani, D. J. Yoo, *J. Membr. Sci.* **2018**, *555*, 497.
[31] F. Tuerxun, K. Yamamoto, T. Mandai, Y. Tateyama, K. Nakanishi, T. Uchiyama, T. Watanabe, Y. Tamenori, K. Kanamura, Y. Uchimoto, *J. Phys. Chem. C* **2020**, *124*, 28510.
[32] R. Mohtadi, F. Mizuno, *Beilstein J. Nanotechnol.* **2014**, *5*, 1291.
[33] J. Muldoon, C. B. Bucur, A. G. Oliver, T. Sugimoto, M. Matsui, H. S. Kim, G. D. Allred, J. Zajicek, Y. Kotani, *Energy Environ. Sci.* **2012**, *5*, 5941.
[34] J. A. Riddick, W. B. Bunger, T. K. Sakano, Organic *Solvents: Physical Properties and Methods of Purification.* 4th edition, John Wiley and Sons: New York, **1986**, p. 167–172.
[35] D. R. Lide, *Boca Rat. CRC Handbook of Chemistry and Physics*, CRC press, **2004**, p. 6–157.
[36] T. Watkins, D. A. Buttry, *J. Phys. Chem. B* **2015**, *119*, 7003.
[37] T. Kimura, K. Fujii, Y. Sato, M. Morita, N. Yoshimoto, *J. Phys. Chem. C* **2015**, *119*, 18911.
[38] S. Y. Ha, Y. W. Lee, S. W. Woo, B. Koo, J. S. Kim, J. Cho, K. T. Lee, N. S. Choi, *ACS Appl. Mater. Interfaces* **2014**, *6*, 4063.
[39] Y. Chen, S. A. Freunberger, Z. Peng, F. Bardé, P. G. Bruce, *J. Am. Chem. Soc.* **2012**, *134*, 7952.
[40] K. M. Anilkumar, B. Jinisha, M. Manoj, S. Jayalekshmi, *Eur. Polym. J.* **2017**, *89*, 249.
[41] J. Evans, C. A. Vincent, P. G. Bruce, *Polymer* **1987**, *28*, 2324.

Manuscript received: September 19, 2023
Revised manuscript received: October 24, 2023
Accepted manuscript online: October 27, 2023
Version of record online: ■■, ■■

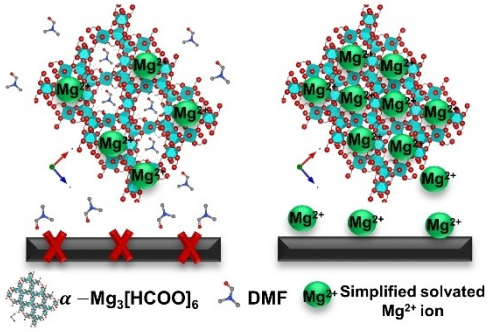

Dr. H. K. Hassan, P. Hoffmann, Prof. T. Jacob**

1 – 14

Effect of Guest Solvents on the Ionic Conductivity and Electrochemical Performance of Metal-Organic Framework-Based Magnesium Semi-Solid Electrolytes

The image shows how the complete evacuation of a metal organic framework (MOF) from the remaining solvent molecules strongly affects the ability to deposit Mg. Our results reveal that the remaining DMF in the MOF may result in (pseudo) high ionic conductivity values; however, its presence, even at low concentrations, leads to the passivation of Mg electrodes. This should be considered when utilizing MOFs in Mg-ion batteries.